Applied Catalysis B: Environmental 248 (2019) 115–119

Contents lists available at ScienceDirect

Applied Catalysis B: Environmental

journal homepage: www.elsevier.com/locate/apcatb

Photocatalytic behaviors of epitaxial $BiVO_4$ (010) thin films

Guoqiang Li[a,*], Qianyun Shen[a], Zhenzhong Yang[b], Shiwen Kou[a], Feng Zhang[a], Weifeng Zhang[a], Haizhong Guo[c], Yingge Du[b,*]

[a] Henan Key Laboratory of Photovoltaic Materials, Henan University, Kaifeng, 475004, PR China
[b] Physical Sciences Division, Pacific Northwest National Laboratory, Richland, WA, 99352, USA
[c] School of Physical Engineering, Zhengzhou University, Zhengzhou, 450001, PR China

ARTICLE INFO

Keywords:
Bismuth vanadate
Substrate
Epitaxial thin film
Photocatalysis

ABSTRACT

Photocatalytic studies performed on well-defined epitaxial thin films and heterostructures allow the direct investigation of crystallographic-dependent reactivity, and can provide fundamental insights into the reaction mechanisms. In this work, we show that phase-pure, monoclinic $BiVO_4$ nanoislands with a truncated pyramid shape with the (010) top surface and {110} sidewalls can be grown on (001)-oriented yttria-stabilized zirconia (YSZ) substrates with an epitaxial relationship of $BiVO_4$(010)[001] // YSZ(001)[100]. The resulting nanostructures show a strong size-dependent mass-normalized photocatalytic activity, with highly dispersed nanoislands at low coverage being the most active. $Pb(NO_3)_2$ photooxidation or photoreduction reactions can be controlled in aqueous solution with and without adding $NaIO_3$ as a electron scavenger, leading to the selective deposition of PbO_2 or Pb on {110} or (010) surfaces of $BiVO_4$, respectively.

1. Introduction

Bismuth vanadate ($BiVO_4$, BVO), with a monoclinic scheelite structure (a = 5.1966 Å, b = 11.7044 Å, c = 5.0935 Å, and β = 90.383°), has attracted great interests due to its superior photocatalytic activities, making it an ideal candidate for use as high performance photocatalysts for visible light-driven water splitting and photoanode in photoelectrochemical cells [1–9]. In order to increase its efficiency, improve charge transport properties, and suppress electron-hole recombination processes, composition and/or morphology tuning have been explored [7,10–15]. In addition, for BVO, researchers have discovered the behaviors of photo-generated carries are facet dependent [14,16–20]. Li et al. demonstrated that faceted BVO crystals with exposed {010} and {110} surfaces are capable of assisting charge separation owing to the difference in energy levels of different facets [16]. Tachikawa et al. found that the trapped holes are preferentially located on the lateral {110} facets of the BVO crystal, while the electrons are uniformly distributed on both facets [18]. Rohrer et al. found that the photochemical reduction of Ag^+ is strongly favored on BVO (010) surfaces (indexed in group C2/c), and the oxidation of Pb^{2+} occur preferentially on surfaces that are perpendicular to (010). [20] Consequently, tuning the proportion of (010) facet was perposed to get a higher effeciency of BVO [12,13,21]. Recently, Schottky-junction on different facets of BVO were formed in aid of polymer [22]. It should be noted that most specimens used in previous studies show preferred {010} and {110} surfaces, and the charge transfer and separation between these two facets have been proposed to play an important role, leading to facet-specific activity towards oxidation/reduction reactions [16,18,17–20,23]. Heteroepitaxial growth techniques not only enable an accurate control over thickness, structure morphology, and surface orientation, but also allow interfacial engineering through the substrate support, which can tune the strain state and electronic structure of the resultant thin films and nanostructures [24–27]. Therefore, it is of great interest to explore whether similar charge transfer processes occur in epitaxial structures with distinct (010) and (110) facets.

For BVO, it has been demonstrated that epitaxial thin films can be grown on (001)-oriented yttria-stabilized zirconia (YSZ (001)) substrates by molecular-beam epitaxy (MBE) [28], chemical vapor deposition (CVD) [29], and pulsed laser deposition (PLD) [30,31]. Stoughton et al. first reported that single-phase monoclinic BVO epitaxial films can be grown on YSZ (001) with an actual Bi:V flux ratio of 31.5 at a substrate temperature of 700 °C by MBE due to the Bi flux being absorption controlled [28]. Archana et al. demonstrated that at lower growth temperature (500–550 °C) can lead to high quality epitaxial BVO films by CVD [29]. Rettie et al. showed that the stoichiometric BVO epitaxial films requires a nonstoichiometric target (Bi:V = 6:1) but at a lower (at 600 °C) temperature by PLD [30]. Van et al. prepared the epitaxial thin film on YSZ(001) substrate at 550 °C

* Corresponding authors.
E-mail addresses: gqli1980@henu.edu.cn (G. Li), Yingge.Du@pnnl.gov (Y. Du).

https://doi.org/10.1016/j.apcatb.2019.02.028
Received 20 July 2018; Received in revised form 1 December 2018; Accepted 12 February 2019
Available online 12 February 2019
0926-3373/

under an oxygen pressure of 250 mTorr [31]. Recently, more complex heterostructures have been fabricated that integrate multi-layers, such as BVO/WO_3/$SrRuO_3$/$SrTiO_3$(001), and BVO/Lu_2O_3/ITO/YSZ by PLD [31–37]. However, the preparation details vary a lot, (e.g., a ~150 °C difference in the substrate temperature and large variation in the target stoichiometry), which can contribute to the structural and chemical differences in the resultant films.

In this paper, we show the phase-pure monoclinic BVO epitaxial nanostructured thin films can be synthesized by pulsed laser deposition. The composition, morphology, and chemical state were investigated by X-ray diffraction (XRD), scanning transmission electron microscopy (STEM), atomic force microscopy (AFM), and X-ray photoelectron spectroscopy (XPS). The initially growth follows a Volmer-Weber mode, leading to oriented BVO nanoislands. Thickness dependent studies show that the highly dispersed nanoislands at low coverage has the highest mass-normalized catalytic activity. The behaviors of photo-generated carriers were probed by reacting with $AgNO_3$ or $Pb(NO_3)_2$ aqueous solution under full arc irradiation of Xe lamp. We show that due to the unique band structure of BVO, the photo-oxidation and -reduction reactions of $Pb(NO_3)_2$ can be controlled using $NaIO_3$ as a electron scavenger, leading to facet-specific deposition of Pb-containing co-catalyst.

2. Experimental

2.1. Sample preparation

The BVO thin films were deposited on YSZ (001) substrates by PLD. Ceramic targets were made by the solid-state methods from powders of bismuth oxide (Bi_2O_3) and vanadium oxide (V_2O_5) with the nominal atomic ratio of Bi to V at 6 and real atomic ratio of Bi to V at 5.4 as determined by inductively coupled plasma optical emission spectrometer (ICP-OES). BVO films with nominal thicknesses ranging from 20 to 45 nm were epitaxially grown on YSZ (001) by PLD. Laser ablation was performed at a repetition rate of 1 Hz and an energy density of 42 mJ/cm^2 with a 248 nm KrF excimer. The substrate temperature used in this work was 680 °C, and the O_2 partial pressure was kept at 7.8 mTorr during growth.

2.2. Material characterization

The crystal structures of BVO films were determined by an X-ray diffractometer with Cu Kα radiation (λ = 0.154145 nm) in θ-2θ mode. The surface morphology and epitaxial relationship were determined by AFM (Bruker multimode 8.0) and scanning transmission electron microscopy (STEM, FEI Titan 80–300). X-ray photoelectron spectroscopy (XPS, Thermo ESCALAB 250, USA) were collected using monochromatic Al Kα x-rays ($h\nu$ = 1486.6 eV) at normal emission. The binding energy was referenced to the C 1 s peak at 284.6 eV.

2.3. Evaluation of photocatalytic activity

The photocatalytic activities of the as-prepared BVO thin films were evaluated by the rhodamine B (RhB) decolorization under full arc irradiation using a 300-W Xe lamp (light intensity ~3.8 mW/cm^2). The photocatalytic reaction was carried out over the samples within a 1 cm^2 area in a 1 mL RhB solution in a sealed quartz cuvette with the light path length of 3 mm. There was no stirring during irradiation, except shaking before the absorbance was measured. The initial concentration of RhB solution was 10 mg L^{-1}. After 30-min dark-reaction, the absorption spectra variations of the RhB were *in-situ* recorded at the intervals of 20 min using a UV–vis spectrophotometer (UV2550, Shimadzu, Japan).

2.4. Precipitation of nanoparticles due to oxidation or reduction reactions

The thin film samples were placed in an O-ring on a glass filled with 0.115 M $AgNO_3$ or $Pb(NO_3)_2$ aqueous solution. A quartz slip was put on top of the O-ring to create a flat and uniform surface for illumination. Samples were illuminated from the topside using Xe lamp equipped with an optical fiber and the intensity of ~30 μW/cm^2, and the exposure time was 7 s. After exposure, the sample was rinsed in water to avoid the precipitation of residual reagents before dried by air.

2.5. Photocatalytic oxygen and hydrogen evolution

Photocatalytic oxygen (hydrogen) evolution were carried out in an aqueous $Pb(NO_3)_2$ solution (an aqueous methanol solution) under full arc irradiation of 300-W Xe lamp. Typically, the sample was placed in the reaction solution in an outer-irradiation type reactor with quartz window. The cocatalyst Pt was loaded by photodeposition during H_2 evoluiton. The amount of O_2 (H_2) evolved were determined with a gas chromatograph equipped with a thermal conductivity detector (TCD).

3. Results and discussion

Using PLD, we explored the compositional range (Bi:V ratio from 1:1 to 7:1) of BVO target and deposition parameters, including oxygen partial pressure, deposition rate, and substrate temperature to map out the conditions leading to stoichiometric BVO [38]. In this work, we show that stoichiometric, faceted BVO nanoislands can be grown using a 5.4:1 (Bi:V) target at a substrate temperature of 680 °C on YSZ(001). Due to the island growth mode and Bi being absorption controlled during deposition, we calculated the nominal thickness of each film based on *ex situ* AFM measurement. Fig. 1(a) shows an XRD *θ-2θ* scan of a BVO film with a 13 nm nominal thickness grown on YSZ (001). It is

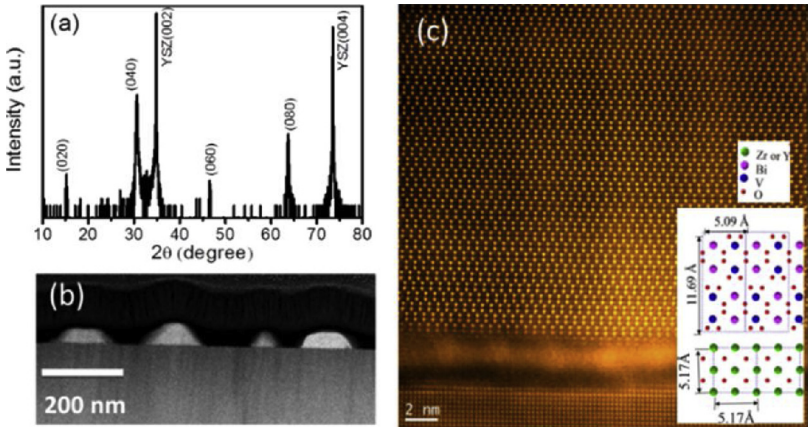

Fig. 1. (a) XRD $\theta - 2\theta$ scan, (b) a low-magnification TEM image, and (c) a high resolution HAADF-STEM images for a BVO film grown on YSZ(001).

noted that the indices used to identify surface planes depend on the symmetry, choice of axis, and unit cell selection. Two choices were adopted in previous studies: one is the modern crystallo-graphic conventions, the longest axis is along b and the space group is C2/c (No. 15); the other is to preserve the relationship between the monoclinic cell and the more idealized tetragonal structure, with the longest axis being c and the group being I2/b [20]. In this work, we adopted the first to be consistent with the description for photocatalytic activity [12,13]. Besides the (002) and (004) reflections of YSZ substrate, the (020), (040), (060) and (080) reflections of BVO were observed in the sample, indicating the phase-pure, monoclinic BVO was formed. Note the (020) reflection is forbidden in tetragonal BVO, only belongs to the monoclinic BVO [28,30]. The lattice constant along b axis is calculated to be 11.6616 Å from the (040) reflection, which are slightly smaller than its bulk value (11.7044 Å), most likely due to the in-plane tensile strain (+1.0%) [28]. From the TEM image as shown in Fig. 1(b), the islands with ~150 nm wide and ~30 nm thickness appear to have a truncated pyramid shape, with {110} sidewalls, similar to the shape of previously synthesized nanoparticles as those are the low surface free energy planes [16,17,28,39].

The interface and epitaxial orientation relationship between BVO and YSZ were investigated by scanning transmission electron microscopy (STEM), as shown in Fig. 1(c). The cross-sectional high-angle annular dark field (HAADF) STEM image reviewed along [100] direction reveals that even though the film/substrate interface contains an amorphous (~3 nm) layer, the projection of the atom positions corresponds well with the crystallographic model of the targeted epitaxial alignment: $BiVO_4$(010)[001] // YSZ(001)[100], which is consistent with previous report [28]. The elemental electron energy loss spectroscopy (EELS) mapping (see Figures S1 in Electronic supporting information (ESI)) shows that the amorphous layer contains Bi, V and O. Such an amorphous layer is also found in PLD grown BVO films by Huang et al. which was ascribed to strain relaxation at interface [32]. The STEM and EELS results also show that the BVO film growth is in Volmer-Weber mode, i.e., three-dimensional islands nucleate and grow directly on the surface of the substrate without a wetting layer.

The growth process was revealed by investigating the morphology changes with deposition time by AFM, as shown in Fig. 2(a). Our AFM offers precise measurement in height (sub-nanometer), but the lateral resolution is in the range of a few nm, so the truncated pyramid shape of the nanoislands was not as evident as under TEM. Nonetheless, well-separated nano-islands (10~22 nm in-lateral size and 2~4 nm in height) are found after 1 min deposition (see Figure S2 in ESI), which evolve to large particles (50~400 nm in-lateral size) with significantly decreased density after subsequent depositions. Even after 60 min, there are still visible gaps between isolated islands. The XPS line survey scan (Figure S3 in ESI) contains obvious Zr 3p signals from the substrates, indicating that the substrates are not covered completely, and the BVO growth is Volmer-Weber mode [28]. The average lateral size and height of the islands were estimated from the AFM images, as shown in Fig. 2(b). The islands' lateral size is found to increase much faster than that of the height (out of plane, thickness). We can estimate the total volume of islands using the size and height and calculate the nominal thicknesses for different deposition times, as shown in Fig. 2(c). The nominal thickness of BVO increases monotonically with the deposition time. Typically, in Volmer–Weber growth, adatom–adatom interactions are stronger than those of the adatom with the surface, leading to the formation of three-dimensional islands. At the beginning, many BVO nucleation sites are small and close to the critical size. Those metastable nucleation centers can go through coalesce, Ostwald ripening, or disintegration [40].

The photocatalytic activity was evaluated from the photocatalytic decolorization of rhodamine B (RhB) with a setup similar to our previous reports [41–43]. When the reagent solution is dilute, the reaction rate (r) can be expressed as $r = kC$, where, k is the apparent rate constant, and C is the instantaneous concentration of the reactant. Taking into consideration of the different morphologies, roughness and mass of these films, to fairly compare the activity, the rate constant per volume of samples prepared under different deposition times are calculated, and plotted in Fig. 2(d). The 1 min sample has the highest catalytic activity/BVO volume, suggesting isolated nanoislands with high density are the most efficient, similar to noble metal catalysts [44,45]. Thus, nanostructuring BVO islands to control their size, density, and distribution should lead to higher performance. Stoughton et al. pointed out that higher Bi:V ratios were needed at higher substrate temperatures [28]. It can be inferred that using a lower (e.g., 3:1 or 4:1) Bi:V ratio target should require a lower substrate temperature to form phase-pure BVO as less Bi desorption is needed. Lowering the growth temperature will lead to a shorter diffusion length, which should result in smaller island with a higher density. Alternatively, using alternative substrates with a larger lattice mismatch may also promote and stabilize island growth. Moreover, the 1 min sample has the higher catalytic activity for DCP degradation in which the dye-sensitized effect could be exclude (Figure S4 in ESI). And the $^{\cdot}OH$ and hole are the main oxidizing species judging from the results of control experiments of adding several kinds of scavengers (Figure S5 in ESI), which agrees well with the previous report [46].

We further studied the behaviors of photogenerated carriers using $AgNO_3$ or $Pb(NO_3)_2$ in aqueous solution as probes under full arc irradiation of Xe lamp as previously reported [16]. Fig. 3a-c show the AFM images of BVO surfaces before and after the reactions. The surfaces of pristine BVO are free of nanoparticles, as shown in Fig. 3(a). After reacting with $AgNO_3$ aqueous solution, Ag nanoparticles were observed preferentially on the (010) surface of BVO, as displayed in Fig. 3(b) [16]. It should be noted that similar to previous studies, $NaIO_3$ was initially added here as an electron acceptor to facilitate the photo-oxidation of $Pb(NO_3)_2$, leading to the deposition of PbO_2 on {110} facets, as shown in Fig. 3(c).

We further examined BVO photocatalytic reactions of $Pb(NO_3)_2$ on BVO without $NaIO_3$. In this case, nanoparticles were observed preferentially on the (010) surface of BVO (Fig. 3(d)), significantly different from that in presence of $NaIO_3$. Previous theoretical calculation results suggested that electrons prefer to accumulate on the (010) surfaces, whereas holes like to accumulate on the (110) surfaces during a photocatalytic process [23]. The particle on (010) should be originated from the electron, which means that the particles result from the photoreduction. The electrode potential of Pb^{2+} reduction to Pb is -0.126 eV (vs. normal hydrogen electrode (NHE)), as shown in Fig. 3(e) [20]. Usually, the valence band top of BVO located at 2.5 eV vs. NHE, taking consideration of the optical band gap of 2.59 eV of BVO nanostructured film (Fig. 3(f), which is in agreement with those reported by Stoughton (2.56 eV) and Archana et al (2.57 eV), but slight smaller than those reported by Mullins (2.65 eV) and Chu et al (2.7 eV) [28–31]), the conduction band bottom is ~ -0.09 eV vs. NHE, close to that of Pb^{2+}/Pb. When UV light is used to excite the BVO, the photogenerated electrons can reduce Pb^{2+} to Pb, and the holes will oxidize H_2O to produce oxygen. To test the above hypothesis, we used $Pb(NO_3)_2$ as electron sacrificial reagent, and indeed found the oxygen evolved from the system as shown in Fig. 3(g). On the other hand, hydrogen was observed using Pt as cocatalyst and methanol as a hole scavenger (Fig. 3(g)), confirming that the conduction band bottom is more negative that the energy level of H^+/H_2 (0 eV vs NHE). Our results reveal that the Pb^{2+} could be oxidized or reduced by controlling the electron acceptors in the reaction system. Moreover, we investigated the photocatalytic activity of the BVO with deposited cocatalyst PbO_2 on different crystal facets. The sample deposited PbO_2 on (010) shows the higher activity for RhB degradation (Figure S6 in ESI).

4. Conclusions

We have shown that epitaxial BVO (010) nanostructured thin films can be grown on YSZ (001) by PLD in a Volmer-Weber mode. Our work

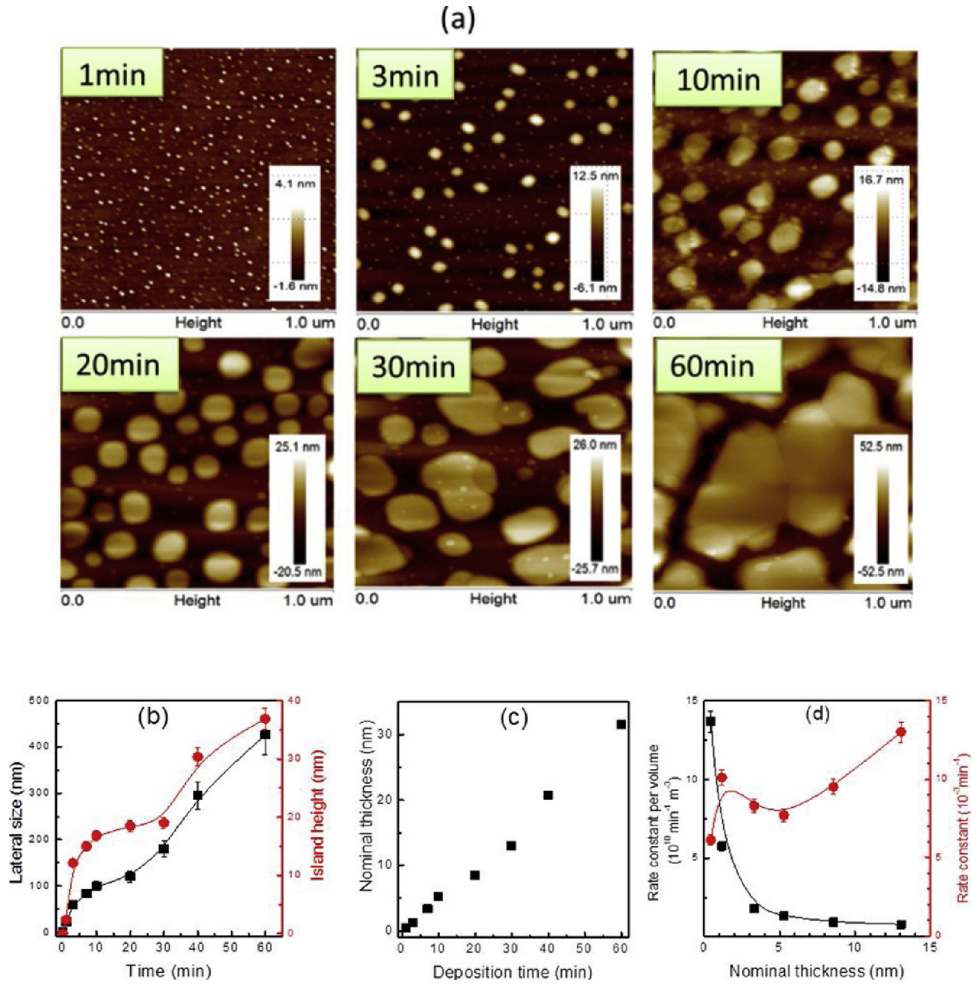

Fig. 2. (a) AFM images and (b) average lateral size and height of BVO islands, (c) nominal thickness of BVO films prepared under different deposition times, and (d) rate constant per volume (square) and rate constant (circle) of RhB degradation over BVO films varied with the nominal thickness.

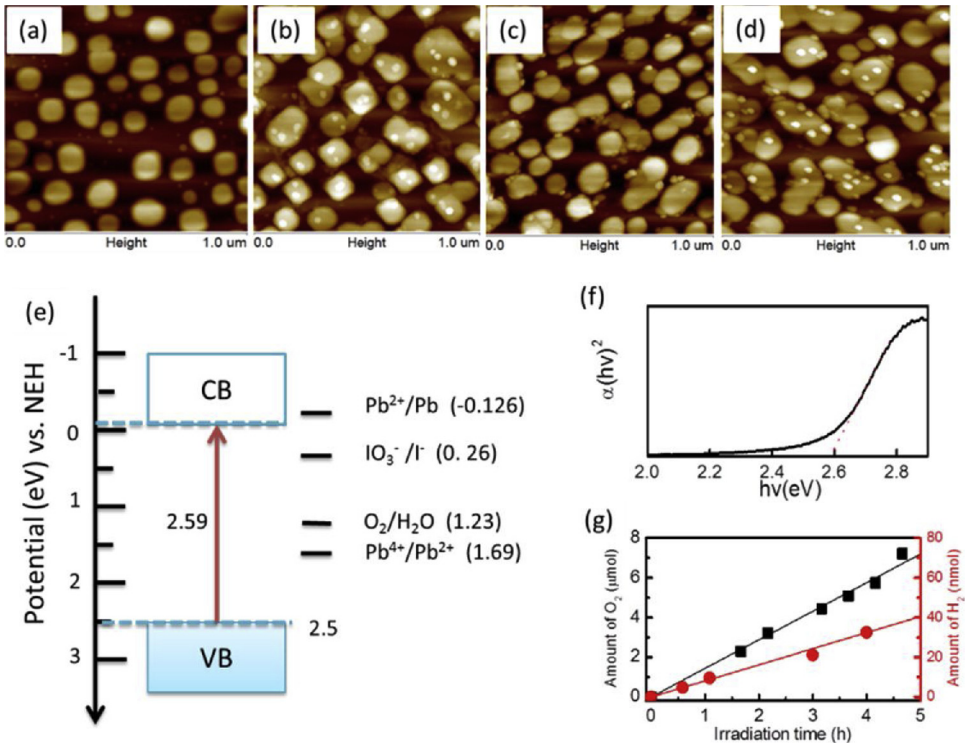

Fig. 3. AFM images of BVO nanoislands with a 10 nm nominal thickness before (a), after reaction with $AgNO_3$ aqueous solution (b), after reaction with $Pb(NO_3)_2$ aqueous solution with (c) and without (d) IO- 3 which accepts electrons, respectively. Energy level diagram showing the band edge positions and redox potentials in $Pb(NO_3)_2$ solution (e). Tauc plot obtained from UV–vis absorption spectra (f). Oxygen and hydrogen evolution vs. irradiation time over BVO nanoislands using $Pb(NO_3)_2$ (0.115 M) as electron scavenger and methanol (25 vol%) as hole scavenger (g).

suggests that the photocatalytic performance of BVO epitaxial heterostructures show a strong size dependent effect, with highly dispersed, nano-sized islands being most active. Different from previous experiments performed on nanoparticles, we show that the reduction of Pb^{2+} occur on the (010) surface of BVO by UV light excitation without any additional electron scavenger. Our results demonstrated that the same cocatalyst can be loaded on different facets of the same photocatalyst, which can affect the photocatalytic performance.

Acknowledgements

G Li acknowledges the support by the Program for Science Technology Innovation Talents in Universities of Henan Province, China (17HASTIT014), the Young Core Instructor Foundation from the Education Commission of Henan Province (2015GGJS-021). Data analysis and TEM work performed by Z.Y. and Y.D. are supported by the U.S. Department of Energy (DOE), Office of Science, Office of Basic Energy Sciences, Early Career Research Program. A portion of the work was performed using EMSL (grid.436923.9), a DOE Office of Science User Facility sponsored by the Office of Biological and Environmental Research.

Appendix A. Supplementary data

Supplementary material related to this article can be found, in the online version, at doi:https://doi.org/10.1016/j.apcatb.2019.02.028.

References

[1] Y. Kuang, Q. Jia, H. Nishiyama, T. Yamada, A. Kudo, K. Domen, A front-illuminated nanostructured transparent BiVO4 photoanode for & 2% efficient water splitting, Adv. Energy Mater. 6 (2016) 1501645.
[2] K. Sivula, R. van de Krol, Semiconducting materials for photoelectrochemical energy conversion, Nat. Rev. Mater. 1 (2016) 15010.
[3] A. Kudo, K. Omori, H. Kato, A novel aqueous process for preparation of crystal form-controlled and highly crystalline BiVO4 powder from layered vanadates at room temperature and its photocatalytic and photophysical properties, J. Am. Chem. Soc. 121 (1999) 11459–11467.
[4] B.J. Trześniewski, I.A. Digdaya, T. Nagaki, S. Ravishankar, I. Herraiz-Cardona, D.A. Vermaas, A. Longo, S. Gimenez, W.A. Smith, Near-complete suppression of surface losses and total internal quantum efficiency in BiVO4 photoanodes, Energy Environ. Sci. 10 (2017) 1517–1529.
[5] D.K. Lee, K.-S. Choi, Enhancing long-term photostability of BiVO4 photoanodes for solar water splitting by tuning electrolyte composition, Nat. Energy 3 (2018) 53–60.
[6] I.D. Sharp, J.K. Cooper, F.M. Toma, R. Buonsanti, Bismuth vanadate as a platform for accelerating discovery and development of complex transition-metal oxide photoanodes, ACS Energy Lett. 2 (2017) 139–150.
[7] T.W. Kim, K.S. Choi, Nanoporous BiVO4 photoanodes with dual-layer oxygen evolution catalysts for solar water splitting, Science 343 (2014) 990–994.
[8] W.J. Luo, Z.S. Yang, Z.S. Li, J.Y. Zhang, J.G. Liu, Z.Y. Zhao, Z.Q. Wang, S.C. Yan, T. Yu, Z.G. Zou, Solar hydrogen generation from seawater with a modified BiVO4 photoanode, Energy Environ. Sci. 4 (2011) 4046–4051.
[9] Y.C. Qiu, W. Liu, W. Chen, W. Chen, G.M. Zhou, P.C. Hsu, R.F. Zhang, Z. Liang, S.S. Fan, Y.G. Zhang, Y. Cui, Efficient solar-driven water splitting by nanocone BiVO4-perovskite tandem cells, Sci. Adv. 2 (2016) 8.
[10] S. Sun, W. Wang, D. Li, L. Zhang, D. Jiang, Solar light driven pure water splitting on quantum sized BiVO4without any cocatalyst, ACS Catal. 4 (2014) 3498–3503.
[11] X. Chang, T. Wang, P. Zhang, J. Zhang, A. Li, J. Gong, Enhanced surface reaction kinetics and charge separation of p-n heterojunction Co3O4/BiVO4 photoanodes, J. Am. Chem. Soc. 137 (2015) 8356–8359.
[12] C.W. Kim, Y.S. Son, M.J. Kang, D.Y. Kim, Y.S. Kang, (040)-Crystal facet engineering of BiVO4 plate photoanodes for solar fuel production, Adv. Energy Mater. 6 (2016) 1501754.
[13] H.L. Tan, X. Wen, R. Amal, Y.H. Ng, BiVO4 {010} and {110} relative exposure extent: governing factor of surface charge population and photocatalytic activity, J. Phys. Chem. Lett. 7 (2016) 1400–1405.
[14] J.-W. Jang, D. Friedrich, S. Müller, M. Lamers, H. Hempel, S. Lardhi, Z. Cao, M. Harb, L. Cavallo, R. Heller, R. Eichberger, R. van de Krol, F.F. Abdi, Enhancing charge carrier lifetime in metal oxide photoelectrodes through mild hydrogen treatment, Adv. Energy Mater. 7 (2017) 1701536.
[15] Y. Wei, J. Su, X. Wan, L. Guo, L. Vayssieres, Spontaneous photoelectric field-enhancement effect prompts the low cost hierarchical growth of highly ordered heteronanostructures for solar water splitting, Nano Res. 9 (2016) 1561–1569.
[16] R.G. Li, F.X. Zhang, D.G. Wang, J.X. Yang, M.R. Li, J. Zhu, X. Zhou, H.X. Han, C. Li, Spatial separation of photogenerated electrons and holes among {010} and {110} crystal facets of BiVO4, Nat. Commun. 4 (2013) 1432.
[17] J. Zhu, F. Fan, R. Chen, H. An, Z. Feng, C. Li, Direct imaging of highly anisotropic photogenerated charge separations on different facets of a single BiVO4 photocatalyst, Angew. Chem. Int. Ed. 54 (2015) 9111–9114.
[18] T. Tachikawa, T. Ochi, Y. Kobori, Crystal-face-dependent charge dynamics on a BiVO4Photocatalyst revealed by single-particle spectroelectrochemistry, ACS Catal. 6 (2016) 2250–2256.
[19] J. Zhu, S. Pang, T. Dittrich, Y. Gao, W. Nie, J. Cui, R. Chen, H. An, F. Fan, C. Li, Visualizing the nano cocatalyst aligned electric fields on single photocatalyst particles, Nano Lett. 17 (2017) 6735–6741.
[20] R. Munprom, P.A. Salvador, G.S. Rohrer, The orientation dependence of the photochemical reactivity of BiVO4, J. Mater. Chem. A 3 (2015) 2370–2377.
[21] S.M. Thalluri, M. Hussain, G. Saracco, J. Barber, N. Russo, Green-synthesized BiVO4 oriented along {040} facets for visible-light-driven ethylene degradation, Ind. Eng. Chem. Res. 53 (2014) 2640–2646.
[22] C. Zhou, S. Wang, Z. Zhao, Z. Shi, S. Yan, Z. Zou, A facet-dependent Schottky-junction electron shuttle in a BiVO4 {010}-Au-Cu2O Z-scheme photocatalyst for efficient charge separation, Adv. Funct. Mater. (2018) 1801214.
[23] J. Hu, W. Chen, X. Zhao, H. Su, Z. Chen, Anisotropic electronic characteristics, adsorption, and stability of low-index BiVO4 surfaces for photoelectrochemical applications, ACS Appl. Mater. Inter. 10 (2018) 5475–5484.
[24] G. Li, T. Varga, P. Yan, Z. Wang, C. Wang, S.A. Chambers, Y. Du, Crystallographic dependence of photocatalytic activity of WO thin films prepared by molecular beam epitaxy, Phys. Chem. Chem. Phys. 17 (2015) 15073–15462.
[25] G.Q. Li, Z.G. Yi, H.T. Wang, C.H. Jia, W.F. Zhang, Factors impacted on anisotropic photocatalytic oxidization activity of ZnO: surface band bending, surface free energy and surface conductance, Appl. Catal. B Environ. 158-159 (2014) 280–285.
[26] G.Q. Li, Z.G. Yi, Y. Bai, W.F. Zhang, H.T. Zhang, Anisotropy in photocatalytic oxidization activity of NaNbO3 photocatalyst, Dalton Trans. 41 (2012) 10194–10198.
[27] K.H.L. Zhang, G. Li, S.R. Spurgeon, L. Wang, P. Yan, Z. Wang, M. Gu, T. Varga, M.E. Bowden, Z. Zhu, C. Wang, Y. Du, Creation and ordering of oxygen vacancies at WO3-delta and perovskite interfaces, ACS Appl. Mater. Interfaces 10 (2018) 17480–17486.
[28] S. Stoughton, M. Showak, Q. Mao, P. Koirala, D.A. Hillsberry, S. Sallis, L.F. Kourkoutis, K. Nguyen, L.F.J. Piper, D.A. Tenne, N.J. Podraza, D.A. Muller, C. Adamo, D.G. Schlom, Adsorption-controlled growth of BiVO4 by molecular-beam epitaxy, Apl. Mater. 1 (2013) 042112.
[29] P.S. Archana, Z. Shan, S. Pan, A. Gupta, Photocatalytic water oxidation at bismuth vanadate thin film electrodes grown by direct liquid injection chemical vapor deposition method, Int. J. Hydrogen Energ. 42 (2017) 8475–8485.
[30] A.J.E. Rettie, S. Mozaffari, M.D. McDaniel, K.N. Pearson, J.G. Ekerdt, J.T. Markert, C.B. Mullins, Pulsed laser deposition of epitaxial and polycrystalline bismuth vanadate thin films, J. Phys. Chem. C 118 (2014) 26543–26550.
[31] C.N. Van, W.S. Chang, J.-W. Chen, K.-A. Tsai, W.-Y. Tzeng, Y.-C. Lin, H.-H. Kuo, H.-J. Liu, K.-D. Chang, W.-C. Chou, C.-L. Wu, Y.-C. Chen, C.-W. Luo, Y.-J. Hsu, Y.-H. Chu, Heteroepitaxial approach to explore charge dynamics across Au/BiVO4 interface for photoactivity enhancement, Nano Energy 15 (2015) 625–633.
[32] H. Song, C. Li, C.N. Van, H.-J. Liu, R. Qi, R. Huang, Y.-H. Chu, C.-G. Duan, Microstructure evolution with composition ratio in self-assembled WO3–BiVO4 hetero nanostructures for water splitting, J. Mater. Res. 32 (2017) 2790–2799.
[33] H. Song, C. Li, C.N. Van, W. Dong, R. Qi, Y. Zhang, R. Huang, Y.-H. Chu, C.-G. Duan, Role of indium tin oxide electrode on the microstructure of self-assembled WO3-BiVO4 hetero nanostructures, J. Appl. Phys. 122 (2017) 175301.
[34] C.N. Van, T.H. Do, J.-W. Chen, W.-Y. Tzeng, K.-A. Tsai, H. Song, H.-J. Liu, Y.-C. Lin, Y.-C. Chen, C.-L. Wu, C.-W. Luo, W.-C. Chou, R. Huang, Y.-J. Hsu, Y.-H. Chu, WO3 mesocrystal-assisted photoelectrochemical activity of BiVO4, NPG Asia Mater. 9 (2017) e357.
[35] J. Song, J. Cha, M.G. Lee, H.W. Jeong, S. Seo, J.A. Yoo, T.L. Kim, J. Lee, H. No, D.H. Kim, S.Y. Jeong, H. An, B.H. Lee, C.W. Bark, H. Park, H.W. Jang, S. Lee, Template-engineered epitaxial BiVO4 photoanodes for efficient solar water splitting, J. Mater. Chem. A 5 (2017) 18831–18838.
[36] W. Zhang, D. Yan, X. Tong, M. Liu, Ultrathin lutetium oxide film as an epitaxial hole-blocking layer for crystalline bismuth vanadate water splitting photoanodes, Adv. Funct. Mater. 28 (2018) 1705512.
[37] W. Zhang, D. Yan, J. Li, Q. Wu, J. Cen, L. Zhang, A. Orlov, H. Xin, J. Tao, M. Liu, Anomalous conductivity tailored by domain-boundary transport in crystalline bismuth vanadate photoanodes, Chem. Mater. 30 (2018) 1677–1685.
[38] G. Li, S. Kou, F. Zhang, W. Zhang, H. Guo, Target stoichiometry and growth temperature impact on properties of BiVO4 (010) epitaxial thin films, CrystEngComm 20 (2018) 6950.
[39] H.L. Tan, A. Suyanto, A.T.D. Denko, W.H. Saputera, R. Amal, F.E. Osterloh, Y.H. Ng, Enhancing the photoactivity of faceted BiVO4 via annealing in oxygen-deficient condition, Part. Part. Syst. Charact. 34 (2017) 1600290.
[40] Z. Wu, B. Wang, X. Sun, Thin Film Growth, Science Press, Bijing, 2013.
[41] Q. Yu, F. Zhang, G. Li, W. Zhang, Preparation and photocatalytic activity of triangular pyramid NaNbO3, Appl. Catal. B 199 (2016) 166–169.
[42] F. Zhang, Z. Wu, B. Sun, G. Li, W. Zhang, Effect of post-treatment on photocatalytic oxidation activity of (111) oriented NaNbO3 film, Apl. Mater. 3 (2015) 104501.
[43] G.Q. Li, B.Y. Sun, Y.L. Wang, Z. Wu, W.F. Zhang, Origin of difference in photocatalytic activity of ZnO (002) grown on a- and c-Face sapphire, Int. J. Photoenergy (2014) 135725.
[44] B. Hvolbæk, T.V.W. Janssens, B.S. Clausen, H. Falsig, C.H. Christensen, J.K. Nørskov, Catalytic activity of Au nanoparticles, Nano Today 2 (2007) 14–18.
[45] M. Murdoch, G.I. Waterhouse, M.A. Nadeem, J.B. Metson, M.A. Keane, R.F. Howe, J. Llorca, H. Idriss, The effect of gold loading and particle size on photocatalytic hydrogen production from ethanol over Au/TiO(2) nanoparticles, Nat. Chem. 3 (2011) 489–492.
[46] M. Yan, Y. Wu, Y. Yan, X. Yan, F. Zhu, Y. Hua, W. Shi, Synthesis and characterization of novel BiVO4/Ag3VO4 heterojunction with enhanced visible-light-Driven photocatalytic degradation of dyes, ACS Sustain. Chem. Eng. 4 (2015) 757–766.